Accepted Manuscript

Title: Enhanced covalent p-phenylenediamine crosslinked graphene oxide membranes: towards superior contaminant removal from wastewaters and improved membrane reusability

Authors: Vepika Kandjou, Ana M. Perez-Mas, B. Acevedo, M. Hernaez, Andrew G. Mayes, Sonia Melendi-Espina

PII: S0304-3894(19)30793-9
DOI: https://doi.org/10.1016/j.jhazmat.2019.120840
Article Number: 120840

Reference: HAZMAT 120840

To appear in: *Journal of Hazardous Materials*

Received date: 13 February 2019
Revised date: 1 May 2019
Accepted date: 26 June 2019

Please cite this article as: Kandjou V, Perez-Mas AM, Acevedo B, Hernaez M, Mayes AG, Melendi-Espina S, Enhanced covalent p-phenylenediamine crosslinked graphene oxide membranes: towards superior contaminant removal from wastewaters and improved membrane reusability, *Journal of Hazardous Materials* (2019), https://doi.org/10.1016/j.jhazmat.2019.120840

Enhanced covalent p-phenylenediamine crosslinked graphene oxide membranes: towards superior contaminant removal from wastewaters and improved membrane reusability.

Vepika Kandjou[1], Ana M. Perez-Mas[1], B. Acevedo[1], M. Hernaez[1], Andrew G. Mayes[2] and Sonia Melendi-Espina[1,]*

[1] Engineering, Faculty of Science. University of East Anglia, Norwich (UK)

[2] School of Chemistry. Faculty of Science University of East Anglia, Norwich (UK)

[*]Corresponding author: Sonia Melendi-Espina; s.melendi-espina@uea.ac.uk

GRAPHICAL ABSTRACT

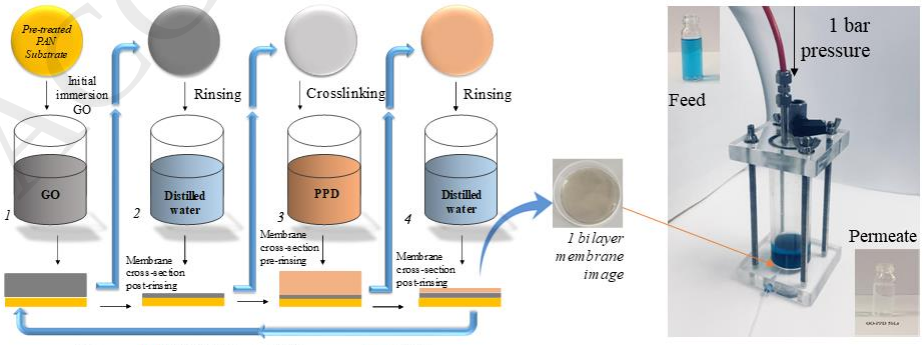

Dip-assisted layer by layer assembly of crosslinked graphene oxide membrane

MB Nanofiltration in a homemade cell

HIGHLIGHTS

- Dip coating and Layer-by-layer have been proven as effective deposition methods.
- Uncrosslinked and PPD crosslinked GO membranes have been successfully fabricated.
- Crosslinker impact is significant in enhanced membrane separation performance.
- Up to 100% MB contaminant removal was achieved for crosslinked membranes.
- PPD-GO crosslinked membranes are suitable to reuse for multiple cycles.

ABSTRACT

The increasing depletion of freshwater necessitates the re-use and purification of wastewaters. Among the existing separation membrane materials, graphene oxide (GO) is a promising candidate, owing to its tunable physicochemical properties. However, the widening of GO membranes pore gap in aqueous environments is a major limitation. Crosslinking agents can be incorporated to alleviate this problem. This study describes a comparative analysis of uncrosslinked and p-Phenylenediamine (PPD) crosslinked GO membranes' water purification performance. Dip-coating and dip-assisted layer-by-layer methods were used to fabricate the uncrosslinked and crosslinked membranes respectively. The covalent interaction between GO and PPD was confirmed by Fourier Transform Infra-Red and X-ray Photoelectron Spectroscopy. The excellent membrane topographical continuity and intactness was assessed by means of Scanning Electron Microscopy, while water contact angle measurements were undertaken to

evaluate and confirm membrane hydrophilicity. The improvement impact of the crosslinker was manifested on the enhancement of the stability and performance of the membranes during nanofiltration tests of aqueous solutions of methylene blue in a homemade nanofiltration cell operated at 1 bar.

KEYWORDS

Graphene oxide, dip coating, layer-by-layer, crosslinker, rejection, methylene blue

1. Introduction

The modern world is currently facing an impending global water crisis, which is fueled by the changing climate, global population increase and the depletion of underground water aquifers [1]. The World Health Organization highlighted that 1.1 billion people lack access to improved drinking water supply [2]. This evidently calls for the re-use of both domestic and industrial waters via improved purification methods and durable materials. From adsorption, distillation to nanofiltration, different water purification methods have been deployed depending on the nature and size of the particulates being separated [3-5]. Among these different purification methods, nanofiltration offers an advantage of having high rejection rates for smaller sized particulates at high flux rates and lower energy consumption relative to energy intensive separation techniques like reverse osmosis [6]. Conventional polymers like polyamide, polysulfone and poly(ethersulfone) are amongst the most used membranes materials in nanofiltration, but the lack of resistance to corrosion and durability of the membranes is a major limitation [7]. Membrane susceptibility to fouling, which shortens their lifespan, has also been a major limitation to most separation membrane materials [8].

Carbon materials have attracted much attention as potential candidates to overcome these issues. Carbon nanotubes (CNTs) have been explored in nanofiltration and their intrinsic mechanical stability and flexibility suggest that they should be ideal nanofiltration membrane materials [9]. Majumder et al reported a high water flux of several orders higher than the predicted hydrodynamic flow using CNTs [10]. However, their relatively high cost, complexity in fabricating vertically aligned CNTs and large-scale production challenges mean that the use of CNTs in nanofiltration is not feasible now [11, 12].

Graphene, with its high mechanical strength evidenced by a Young's modulus of 1 TPa, 2-dimentionality, high specific surface area and insusceptibility to fouling, is an ideal next generation nanofiltration membrane material [13–15]. Although it is a model membrane material due to its outstanding properties, scaling up the production of a defect free, one atom thick large area graphene is extremely challenging [16, 17]. Furthermore, scalable formation of sub-nanometer pores on pristine graphene membrane for nanofiltration is a cost-intensive process [18–20].

Fortunately, GO, a derivative of graphene with protruding oxygenated functional groups, has emerged as a reasonable graphene substitute pertaining to separation membrane applications [21, 22]. Initial experiments by Nair et al. have paved a way for the use of GO as a separation membrane precursor in water purification [23]. GO can be fabricated cost effectively and therefore can be easily up-scaled to mass production [24, 25]. Furthermore, its possession of oxygenated functional groups enhances its hydrophilicity, limiting membranes' fouling susceptibility [26-29]. This further adds to the materials' chemical activity the ability to be covalently interconnected to molecular compounds which further enhances the properties of fabricated hybrid GO membranes [30-32].

The major drawback to the use of solely GO in membrane separation is the lack of membrane stability during nanofiltration [33]. It has been discovered that GO membranes tend to swell during water purification [33, 34]. This is mostly advocated to the enlargement of the interlayer gap because of the accumulation of water molecules onto the oxygenated functional groups, consequently leading to reduced membrane rejection over time [22]. Several attempts have been made to try to alleviate this major problem. For instance, Abraham et al. used an epoxy encapsulate to physically confine the pore gap of GO membranes [35]. The major limitation to the physical confinement method employed is that scale-up for production of such membranes is a great challenge [35]. Zhang et al. explored covalent crosslinking of GO membranes using ethylenediamine as a crosslinker and the vacuum filtration fabrication method [36]. However, higher GO loading is used and difficulty in controlling membrane thickness relative to layer-by-layer assembly is a limitation for the vacuum filtration method [37]. Elsewhere, attempts to fabricate nanofiltration layer-by-layer assembled membranes have been made [38, 39, 40], however, a comparative investigation of the impact of multilayers of sub-nanometer sized covalent based crosslinked GO membranes via dip-assisted layer-by-layer assembly has not been explored to the authors current knowledge.

Consequently, this study aimed at the enhancement of membrane stability and separation abilities of GO membranes through the introduction of a small, subnanometer-sized covalent crosslinker, on a dip-assisted layer-by-layer basis. This should bond adjacent layers of GO plates together, thus stabilizing the structure during membrane operation. Two sets of GO based membranes were fabricated, uncrosslinked and crosslinked with p-phenylenediamine (PPD). Dip coating method for the uncrosslinked membranes and dip-assisted layer by layer assembly were the fabrication methods explored for the crosslinked membranes in this study.

The explored membrane fabrication methods offer an added advantage of fabrication of continuous membranes with controlled thickness and low material load [38, 39, 40]. Simplicity in operation, together with cost effectiveness are also key benefits of these fabrication methods [40]. The fabrication methods, especially dip-assisted layer-by-layer, offers firmer interconnection between the GO and crosslinker layers, thus avoiding the swelling and enlargement of GO interflake gaps that is a common problem for GO membranes in aqueous environments [37].

The study also addressed the influence of number of layers and bi-layers on the water purification capabilities of the membranes.

2. Materials and methods

2.1 Materials

GO powder was purchased from Graphenea (Spain). The membranes were supported by poly(acrylonitrile) (PAN) filter substrates with 0.2 μm pore size and 47 mm diameter from Sterlitech Corporation (USA).

The crosslinker, p-phenylenediamine (PPD, product code P6001), polyethyleneimine (PEI, product code 03880), potassium hydroxide powder (KOH) and methylene blue (MB, product code M9140) were all purchased from Sigma Aldrich (UK). A bath type sonicator (Fisherbrand FB1505, Elmasonic S30H) enhanced the dispersion of the GO water suspensions and the membranes were fabricated with a rotary dip-coater device (Nadetech Innovations, Spain).

2.2 Crosslinked and uncrosslinked membrane fabrication

2.2.1 Pre-treatment of poly (acrylonitrile) (PAN) substrates

The 0.2 μm pore sized fibrous PAN substrates were first hydroxylated via immersion in 1 M KOH for 30 minutes at 70 °C. This was done to enhance a negative charge via the conversion of the nitriles in the PAN substrates to carboxylic groups [39, 41, 42]. Subsequently, the substrates were rinsed with distilled water and dried prior to immersion in a positively charged 2.0 mg/ml PEI solution for 5 minutes. PEI conferred a positive charge onto the hydroxylated PAN substrates [42]. The positively charged substrates were then rinsed in distilled water to remove excess unattached PEI and then dried prior to membrane fabrication.

2.2.2 Dip-Coating and Dip-Assisted Layer-by-Layer Assembly

Prior to membrane fabrication, 0.5 mg/ml of GO aqueous dispersion was prepared and sonicated for 2 hours to enhance the individuality and dispersion of the GO sheets in water. To analyse the impact of the crosslinker on the performance and stability of the GO membrane, two types of membranes were fabricated. One was the uncrosslinked GO membranes, fabricated via dip-coating method where, following pre-treatment, the PAN substrates were immersed in 0.5 mg/ml GO dispersion solution in a vertical orientation with rinsing and drying between cycles (Figure 1). This was done using 5 minutes immersion time and membranes with 1 and 5 assembly cycles were fabricated.

In the crosslinked membranes, PPD was introduced onto the membranes via dip-assisted layer-by-layer assembly. This was done on an alternating basis with GO, with rinsing and drying after each immersion in GO or PPD (Figure 2). The main basis of this layer-by-layer fabrication was an epoxy ring opening reaction between the amines in PPD and the epoxy group in GO (Figure

3) [31, 43], where a hydroxyl group and a secondary amine are generated. This leaves the other amine group in PPD to interconnect with a subsequent GO sheet in the next assembly.

Subsequently, 1 and 5 bi-layers were assembled using 5 minutes immersion time.

2.3 GO and PPD covalent bonding

A crucial step in this study was to verify the GO-PPD covalent bonding via a chemical reaction at the designated reaction time. Following the preparation of a 0.5 mg/ml of aqueous GO suspension and 2.0 mg/ml of aqueous PPD solution, both were reacted for 5 minutes (which was the membrane fabrication immersion time). The reaction time was controlled by a pH switch through the addition of 97% purity sulphuric acid (H_2SO_4, Sigma Aldrich, product code: 07208) to the reacting mixture, which resulted in the protonation of the reacting entities and hence rendering them unreactive after the addition of the acid [44, 45, 46]. The reacted entities were then centrifuged (Bio-Fuge Primo Heraeus Centrifuge) at 1000 rpm for 10 minutes to collect the centrifuge residue for FTIR and XPS characterizations. The centrifugation was done with rinsing three times with distilled water to remove the excess unreacted entities.

The presence of notable functional groups in GO, PPD and reacted entity were determined by FTIR and XPS. An attenuated total reflectance unit (ATR) equipped PerkinElmer Spectrometer was used for the FTIR analysis while a Kratos Ultra-DLD XPS System (K-Alpha$^+$) was used for the XPS characterizations.

2.4 Contact angle measurements

As it proved impossible to measure the water contact angles on hydrophilic porous PAN substrates due to permeation of pure water through the membranes, uncrosslinked and crosslinked films were similarly fabricated on non-porous silicon-based glass slide substrates to measure the relative water contact angles of the thin films. This was similarly done at 5 minutes immersion time and 1 and 5 layers and bilayers.

To enhance the reliability of the results, an average of 8 contact angle measurements was taken, noting down the standard deviation in error bars. Several pure water drops were introduced to the films in different positions from two different fabrication sets of the same film type.

The water contact angle measurements were subsequently recorded with a DMK 31BF03 camera and the angles were processed by image j software (1.50i/ Java 1.6.0) (Public Domain, BSD-2).

2.5 Membrane performance tests

2.5.1. Nanofiltration setup

Following the fabrication of both crosslinked and uncrosslinked membranes, the membrane performance was evaluated with a 10 mg/l aqueous solution of MB. The tests were carried out at room temperature in a 330 cm^3 dead end homemade filtration cell constructed from poly (methyl methacrylate) (Figure 4), where the membrane was supported by a porous sintered polyethylene disc with an effective area of 13.20 cm^2 and an operation pressure of 1 bar. The cell was sealed with neoprene gaskets.

To enhance the reliability of the results, three membranes of the same type were fabricated and subsequent standard deviation of the nanofiltration results were noted for both the flux and rejection results.

The overall membrane performance was determined through calculation of the permeation flux (F) across the membrane. This was determined from the total permeate volume collected (V) per unit time (t) and membrane effective area (A) (Eq 1).

$$F = V/(A\,t) \qquad \text{Eq (1)}$$

2.5.1. Methylene Blue calibration line.

The membrane rejection, on the other hand, was determined by UV-Vis characterization of the permeate solutions relative to the feed solution. A calibration line relating MB concentrations with absorbance was then established (Eq. 2) in order to have a concentration based MB rejection, as follows:

$$\text{Absorbance (a.u)} = 0.1897\ \text{MB concentration (mg/l)} \qquad \text{Eq (2)}$$

$R^2 = 0.9971$

Percentage rejection [R (%)] was then calculated using equation 3. Where C_p is the permeate concentration and C_f the feed concentration.

$$R\ (\%) = \left(1 - \frac{cp}{cf}\right).100 \qquad \text{Eq (3)}$$

2.6 Continuity of uncrosslinked and crosslinked membranes

The surface coverage and continuity of the fabricated membranes was analysed by a JEOL JSM – 5900 Scanning Electron Microscope, before and after the nanofiltration experiments. Prior to characterization, the membranes were coated with gold using a CC7640 Quorum Technologies Gold Coater.

3. Results and Discussions

3.1 Proof of covalent bonding between GO and PPD.

The significance of the FTIR characterizations was to verify the presence of the notable functional groups in the reacting entity, these being the epoxide in GO and the amine groups in PPD. These are essential for covalent crosslinking of both via an epoxy ring opening reaction as stated previously. A covalent –C-N- bond between GO and PPD is expected following an epoxy ring opening reaction [47, 48].

The loss of the doublet band near 3400 cm^{-1} in the PPD spectrum is evidence for the interconnection of the PPD and GO where the primary amine (1°) in PPD converted to a secondary amine (2°) [47] and a new C-N bond was formed and it is assigned by the stretch at around 1250 cm-1 [49] (Figure 5). The IR spectra also show a small but distinct band at around 1500 cm^{-1}, corresponding with N-H bend [50]. This is present in the reference PPD spectrum (very strong) and it is clearly visible in the reacted entity. However, it is notably absent in the GO spectrum. The appearance of this band corresponds with an evident reduction in the signal at 1060 cm^{-1}, which can be attributable to epoxy C-O bonds [43, 51, 52]. This is in agreement with the XPS results, which show a clear decrease of C(epoxy) (Table 1).

Wide-scan spectra in the binding energy range of approximately 0–1000 eV were obtained to identify the elements present on the surfaces of the GO and the GO-PPD reacted entity to further support the covalent cross-linking.

High resolution spectra were obtained and the carbon and nitrogen spectra were fitted. Five peaks emerged at different binding energies (BE) when the C1s peak was curve fitted, which correspond to C graphitic (BE = 284.3–284.4 eV), C-O in the epoxy bond (BE = 285.6–285.7 eV), C=O in the carbonyl bond (BE = 286.9-287.0), the peak at around 288.9 assigned to the carboxyl bond as well as the π-π* shake-up signal (290.8 eV) typical for sp^2- hybridized carbon. The N(1s) peak was also curve-fitted, emerging five peaks, assigned to N6 from N-pyridine like structures (BE = 398.8-398.4 eV), NC from amides/amines or lactams (BE = 399.9-399.5 eV), N5 from N-pyrrolic (BE = 400.6-400.0 eV), NQ from N-quaternary (BE=401.8-400.9) and the peak at around 405-402 eV assigned to the nitrogen oxides as Pyridine N-Oxide (N-X).

XPS characterizations show a small introduction of nitrogen into material that is completely absent in the starting GO (Table 1). Of this nitrogen, significant signal corresponds to amines/amides. In this case, it relates with the presence of secondary amines due to the epoxy ring opening. Formation of amides is heavily disfavored under the aqueous reaction conditions used, since it is a condensation reaction. Normally acid activation chemistry is required (e.g. as acid chlorides, active esters or similar) to achieve such reactions and even then there is a competitive reaction with water as active nucleophile. Unlike the amide formation reaction, nucleophilic attach of epoxy groups to generate secondary amines is a reaction that readily occurs under mild aqueous conditions. Indeed, such reactions are routinely used to couple

proteins to epoxy-activated polymeric supports for instance. Additionally, if this nitrogen corresponded to amides, there would be a concomitant reduction in COOH signal, but this is the opposite of what the XPS indicates, showing significant increase in COOH.

Of the N present, a large proportion is quaternized/charged. This can be explained through the acid treatment of the material to stop the reaction, which would leave secondary amines charged, but would have no effect on any amides present, since they do not ionize under these conditions, This is a further evidence of amine formation.

3.2 Membrane continuity analysis

The uniformity of coverage of the fabricated membranes is necessary to prove successful membrane fabrication onto the PAN support substrates. To an extent, the characterizations were carried out to give detailed information on the stability and intactness of the fabricated membranes, both before and after nanofiltration tests (the latter shown in Figure 12, after performing the rejection analysis).

Figure 6 shows that there is good coverage for both membrane types from the very first bi-layer. This can be seen further in detail in the subsequent SEM images shown in Figure 7. The membrane coverage increases, as the number of assembly cycles increases from 1 cycle to 5 cycles for both crosslinked and uncrosslinked membranes. This is because of the increase in material accumulation as the number of assembly cycles increases [47]. The coverage is significant for the closing of the fibrous pore gaps in the plain PAN substrates as this gives a good sieving potential for the separation performance of the fabricated membranes [39, 53]. The ability to enhance proper membrane pore size is therefore dependent on the number of dip coating and dip-assisted layer by layer assembly cycles in this regard [54].

3.3 Hydrophilicity analysis

The hydrophilicity of the membranes is a significant characteristic in water purification since the more hydrophilic the membranes are, the less they are susceptible to fouling [27]. Relatively, the crosslinked membranes have lower hydrophilicity compared to the uncrosslinked ones. This is due to the hydrophobic nature of the PPD crosslinker [55, 56]. For the crosslinked membranes, the water contact angle increased from 53.2° to 59.7° with an increase in the number of bi-layers (Figure 8) owing to bigger accumulation of the hydrophobic crosslinker. However, a decrease in the contact angle for the uncrosslinked membranes from 38.2° to 35.2° was observed as the number of layers increased from 1 to 5 due to increased accumulation of the hydrophilic GO. Overall, both crosslinked and uncrosslinked membranes are relatively very hydrophilic as they show low water contact angles and ease permeation of water [57].

3.4 Membrane performance results analysis

3.4.1 Rejection analysis

The fabricated membranes were tested in a lab-scale nanofiltration device to study their performance on the removal of MB. Permeates after passing through each fabricated membrane are displayed in Figure 9, where the decrease in coloration, which symbolizes the removal of MB, is evident.

Across the two membrane types, MB rejection increases with the assembly cycles (Figure 10). The average MB rejection increased from 20.4% to 99.8% for the crosslinked membranes as the number of bi-layers increased from 1 to 5. Comparatively, the uncrosslinked membranes showed

a similar trend, as the GO layers increased from 1 to 5 the rejection increased from 5.1% to 87.4%. It is also evident that the performance of the membranes improved with the addition of the crosslinker. This is indirect evidence that the crosslinker holds the GO nanosheets together through the –C-N- covalent bonds [58] and thus maintains the pore gap in the sub-nanometer range even when wetting occurs.

3.4.2 Flux analysis

The flux decreases as the number of assembly cycles increases for both crosslinked and uncrosslinked membranes (Figure 11). A sharp decrease in flux from the plain PAN to the coated membranes is observed. This is evidence for substrate pore size reduction via GO coverage. Crosslinking also results in decrease in flux, as for similar number of assembly cycles the crosslinked membranes display a lower flux in comparison with the uncrosslinked ones. For instance, 1 layer of uncrosslinked GO on the membrane had a flux of 18.7 $l.m^{-2}.h^{-1}$ while it was 6.2 $l.m^{-2}.h^{-1}$ for the crosslinked one. However, at larger assembly cycles a smaller decrease in flux of only 0.2 $l.m^{-2}.h^{-1}$ was observed (2.0 vs 1.8 $l.m^{-2}.h^{-1}$).

The decrease in flux with the number of assembly cycles is hypothesized to be due to the increase in membrane compactness due to material accumulation. The lengthening of the tortuous path as the number of assembly cycles increases is also significant for the reduction in permeation flux [37]. A likely factor for the observed flux difference between crosslinked and uncrosslinked membranes is that crosslinking maintains a smaller pore-gap, hence the lower flux, while for the uncrosslinked membranes, wetting resulted in enlarged membrane pores and therefore increased flux [33].

Elsewhere, lower fluxes at 10 times higher operation pressure than the one used in this study have been reported; for instance, Aba et al reported a lower flux in the range of 0.58 to 0.60 $l.m^{-2}.h^{-1}$ on the separation of organic dyes at an operation pressure of 10 bars [59]. Thus given the lower pressure of only 1 bar used and the relatively high flux achieved in this study, the significance of the results of this study is apparent.

The molecular size of an individual MB (anhydrous basis) molecule is about 1 nanometer (13.84 Å) [60, 61]. It is smaller than most textile dyes like remazol yellow [60, 62]. These are therefore significant results for the separation of almost all textile dyes and they can be refined further to separate even smaller entities including divalent salts. The ease of fabrication of the membranes, very low GO loading, cost effectiveness and their stability is a step forward in the purification of dye contaminated waters.

3.5 Membrane separation mechanism, operation longevity and reusability

To understand the separation mechanism and operation longevity of the fabricated membranes, the overtime separation of the best performing membrane (PPD crosslinked 5 bi-layers) was analyzed. Continuous operation of the membrane for more than 120 hours at 1 bar showed no decrease in membrane selective separation abilities, however the flux across the membrane considerably diminishes over time (Table 2). The maintenance of a constant rejection throughout the experiment leads to the conclusion that the mechanism at hand is mainly a selective permeation based separation instead of a selective binding based separation [63-67].

The separation mechanism was further evaluated increasing the feed concentration to 125 and 250 mg/l and it was observed that the permeation flux at the high feed concentration decreases drastically at prolonged membrane operation and as the feed concentration increases (Table 3).

This might be attributable to the increased initial adsorption of MB onto the GO membranes via electrostatic attractions between the negatively charged oxygenated functional groups in GO and the positively charged nitrogen containing groups in MB [68]. However, the level of carboxylate functional groups in GO is relatively low, so saturation of these sites would occur quite rapidly, even at low MB concentrations. Very importantly, the presence of aromatic rings in GO and PPD from the membrane and MB also gives rise to $\pi - \pi$ interactions, which are likely to enhance the adsorption of MB onto the membranes in the initial operation stages of the permeation tests [69-72]. Such interactions are strong under aqueous conditions. This in turn narrows the permeation path significantly and thus resulting in a decreased flux across the membrane and high MB rejection at prolonged membrane operation.

The reusability of the membranes was achieved in a facile manner through the rinsing of the 5 bilayers crosslinked membrane after operation in a 15% (v/v) ethanol aqueous solution for 15 minutes. This resulted in the removal of attached MB giving the membranes good operation efficiency post initial use and confirming that MB was adsorbed onto the membrane. It was found out that the nanofiltration performance of the membranes post membrane rinsing was recovered almost to the initial performance, accomplishing a flux of 1.74 $l.m^{-2}.h^{-1}$ (Initial flux = 1.8 $l.m^{-2}.h^{-1}$) and a rejection of 99.2 %. Five cycles of post clogging rinsing of the membranes were performed so the values provided are the average of all the series. Given the more than 120 hours operation longevity of the membranes per cycle before complete clogging and the excellent performance recovery, authors believe that the longevity and reusability of the membranes is thus highly feasible.

The longevity of the membranes paves a way for the implementation of these membranes in water purification. This modification of GO via crosslinking offers a myriad of opportunities for the use of these membrane in other separations. Potentially, this makes GO membranes potential alternatives to the current commercial thin-film membranes like polyamide taking into account the low pressure used in this study.

3.6 Membrane stability

Stability is also a significant membrane characteristic as it governs the re-usability and longevity of the membranes. For that reason, to investigate the integrity of the fabricated membranes, SEM characterizations were also carried out after the nanofiltration experiments and once the membranes were dried. Images are shown in Figure 12.

Images evidently indicate that the uncrosslinked membranes tend to have micrometer-sized cracks as they dry up. This can be promoted by the consolidation of GO nanosheets as the solvent leaves the dispersion during drying [73]. No cracks could be spotted on the crosslinked membranes, demonstrating the influence of the crosslinker on the intactness of the GO-PPD membranes. This is likely a significant factor influencing the observed membrane performance difference between crosslinked and uncrosslinked membranes.

The membrane stability was further investigated through the fabrication of crosslinked and uncrosslinked membranes through the use of a pressure-assisted filtration method. For the uncrosslinked membranes, a 15ml solution of 0.5 mg/ml of GO was filtered through PAN substrates using the homemade nanofiltration cell at a pressure of 3 bars. The crosslinked membranes, on the other hand, were fabricated by first reacting the GO and PPD solution and then filtrating the reacted entities in the same device at the same pressure. The fabricated

membranes were then dried for 24 hours to observe their stability over time under a dry environment (Figure 13).

Similar results regarding membrane stability were observed. Uncrosslinked membranes tend to break and shrink after 24 hours of drying. This phenomenon was ascribed to the drying related shrinkage of the membranes [68, 73]. This further supports the observed micro cracking in dip-coated membranes. The higher material loading in this case results in evident visible cracks and the role of the crosslinker in alleviating the drying induced cracking is evident.

The disentanglement of the uncrosslinked membranes in comparison to the crosslinked membranes can be clearly observed. This validates the previous observation that crosslinking does not only enhance membrane rejection performance but also their stability, longevity, reusability and intactness of GO membranes.

4. Conclusions

In summary, uncrosslinked and PPD crosslinked GO membranes were successfully fabricated using dip-coating and dip-assisted layer by layer fabrication methods. The membrane performance in water purification was proven through the separation of MB via a homemade nanofiltration cell. The rejection increases as the number of assembly cycles increases for both membrane types. Better performance was observed for the crosslinked membranes relative to the uncrosslinked at similar assembly cycles. Through this study, the significance of covalent crosslinking was demonstrated, it was not only manifested in nanofiltration performance but also in enhanced stability and membrane intactness over time. A relatively high flux at an economical 1 bar driving pressure and excellent removal of MB (up to ~100%) was achieved for the crosslinked membranes and the stability and durability of layer by layer GO membranes was

enhanced. The best performing crosslinked membranes also showed good operation longevity at the low operating pressure as they could be operated continuously for more than 120 hours with no reduction in dye rejection. The good membrane reusability achieved also enhances the possibility of the use of covalent based crosslinkers in the fabrication of GO based membranes. The membranes can potentially be used for separation of other organic dyes, bacteria and other microbes; they can also be modified further for other significant separations like desalination.

Acknowledgments

Special thanks the Botswana Government's Ministry of Tertiary Education and Scientific Research and the Top Achievers Scholarship Programme for offering a Scholarship (100159844RA2 – TR. 163096) that aided the carrying out of this work.

References

[1] P. H. Gleick, Water in Crisis: A Guide to the World's Freshwater Resource. Oxford University Press, 1993.

[2] W. World Health Organization, Meeting the MDG drinking water and sanitation, the urban and rural challenge of the decade, Geneva, 2007.

[3] K. Dutta and S. De, Smart responsive materials for water purification: An overview, J. Mater. Chem. A 5 (2017) 22095–22112.

[4] S. Babel and T. A. Kurniawan, Low-cost adsorbents for heavy metals uptake from contaminated water: A review, J. Hazard. Mater. 97 (2003) 219–243.

[5] F. Fu and Q. Wang, Removal of heavy metal ions from wastewaters: A review, J. Environ. Manage. 92 (2011) 407–418.

[6] H. K. Shon, S. Phuntsho, D. S. Chaudhary, S. Vigneswaran, and J. Cho, Nanofiltration for water and wastewater treatment - A mini review, Drink. Water Eng. Sci. 6 (2013) 47–53.

[7] R. J. Petersen, Composite reverse osmosis and nanofiltration membranes, J. Memb. Sci. 83 (1993) 81–150.

[8] L. Braeken, K. Boussu, B. Van Der Bruggen, and C. Vandecasteele, Modeling of the adsorption of organic compounds on polymeric nanofiltration membranes in solutions containing two compounds, ChemPhysChem. 6 (2005) 1606–1612.

[9] L. F. Dumée, K. Sears, J. Schutz, N. Finn, C. Huynh, S. Hawkins, M. Duke and S. Gray, Characterization and evaluation of carbon nanotube Bucky-Paper membranes for direct contact membrane distillation, J. Memb. Sci. 351 (2010) 36–43.

[10] M. Majumder, N. Chopra, and B. J. Hinds, Mass transport through carbon nanotube membranes in three different regimes: Ionic diffusion and gas and liquid flow, ACS Nano 5 (2011) 3867–3877.

[11] M. Yu, H. H. Funke, J. L. Falconer, and R. D. Noble, High density, vertically-aligned carbon nanotube membranes, Nano Lett. 9 (2009) 225-229.

[12] S. Kim, J. R. Jinschek, H. Chen, D. S. Sholl, and E. Marand, Scalable fabrication of carbon nanotube/polymer nanocomposite membranes for high flux gas transport, Nano Lett. 7 (2007) 2806–2811.

[13] A. Geim and K. Novoselov, The rise of graphene, Nat. Mater. 3 (2007) 183–191.

[14] A. Boretti, S. Al-Zubaidy, M. Vaclavikova, M. Al-Abri, S. Castelletto, and S. Mikhalovsky, Outlook for graphene-based desalination membranes, npj Clean Water 1 (2018) article number 5.

[15] Y. Han, Z. Xu, and C. Gao, Ultrathin graphene nanofiltration membrane for water purification, Adv. Funct. Mater. 23 (2013) 3693–3700.

[16] J. R. Werber, C. Osugi, and M. Elimeneck, Materials for next-generation desalination and water purification membranes, Nat. Mater. 1 (2016) article number 16018.

[17] S. P. Surwade, S. N. Smirnov, I. V. Vlassiouk, R. R. Unocic, G. M. Veith, S. Dai and S. M. Mahurin, Water desalination using nanoporous single-layer graphene, Nat. Nanotechnol. 10 (2015) 459–464.

[18] K. S. Novoselov, A.K. Geim, S. V. Morozov, D. Jiang, Y. Zhang, S. V. Dubonos, I. V. Grigorieva and A. A. Firsov, Electric field effect in atomically thin carbon films, Science 306 (2004) 666-669.

[19] C. J. Russo and J. A. Golovchenko, Atom-by-atom nucleation and growth of graphene nanopores, Proc. Natl. Acad. Sci. 109 (2012), 5953–5957.

[20] S. C. O'Hern M. S. H. Boutilier, J. C. Idrobo, Y. Song, J. Kong, T. Laoui, M. Atieh, and R. Karnik, Selective ionic transport through tunable subnanometer pores in single-layer graphene membranes, Nano Lett. 3 (2014) 1234–1241.

[21] R. K. Joshi, P. Carbone, F. C. Wang, V. G. Kravets, A. K. Geim, and R. R. Nair, Precise and ultrafast molecular oxide membranes, Science 343 (2014) 752–755.

[22] R. K. Joshi, S. Alwarappan, M. Yoshimura, V. Sahajwalla, and Y. Nishina, Graphene oxide: The new membrane material, Appl. Mater. Today 1 (2015) 1–12.

[23] R. Nair, H. Wu, A. V. Jayaram, V. Grigorieva, and A. Geim, Unimpeded permeation of water," Science 335 (2012) 442–445.

[24] K. H. Lee, B. Lee, S. Hwang, J. Lee, H. Cheong, O. Kwon, K. Shin, and N. H. Hur, Large scale production of highly conductive reduced graphene oxide sheets by a solvent-free low temperature reduction, Carbon 69 (2014) 327–335.

[25] S. Abdolhosseinzadeh, H. Asgharzadeh, and H. S. Kim, Fast and fully-scalable synthesis of reduced graphene oxide, Sci. Rep. 5 (2015) 1–7.

[26] L. Jin, Z. Wang, S. Zheng, and B. Mi, Polyamide-crosslinked graphene oxide membrane for forward osmosis, J. Memb. Sci. 545 (2018) 11–18.

[27] M. Hu, S. Zheng, and B. Mi, Organic fouling of graphene oxide membranes and its implications for membrane fouling control in engineered osmosis, Environ. Sci. Technol. 50 (2016) 685–693.

[28] C. Zhao, X. Xu, J. Chen, G. Wang, and F. Yang, Highly effective antifouling performance of PVDF/graphene oxide composite membrane in membrane bioreactor (MBR) system, Desalination 340 (2014) 59–66.

[29] H. R. Chae, J. Lee, C. H. Lee, I. C. Kim, and P. K. Park, Graphene oxide-embedded thin-film composite reverse osmosis membrane with high flux, anti-biofouling, and chlorine resistance, J. Memb. Sci. 483 (2015) 128–135.

[30] A. Lerf, H. He, M. Forster, and J. Klinowski, Structure of Graphite Oxide Revisited ‖, J. Phys. Chem. B 102 (1998) 4477–4482.

[31] I. A. Vacchi, C. Spinato, J. Raya, A. Bianco, and C. Ménard-Moyon, Chemical reactivity of graphene oxide towards amines elucidated by solid-state NMR, Nanoscale 8 (2016) 13714–13721.

[32] D. Dreyer, S. Park, C. Bielawski, and R. Ruoff, The chemistry of graphene oxide, R. Soc. Chem. 39 (2010) 228–240.

[33] S. Zheng, Q. Tu, J. J. Urban, S. Li, and B. Mi, Swelling of graphene oxide membranes in aqueous solution: Characterization of interlayer spacing and insight into water transport mechanisms, ACS Nano 11 (2017) 6440–6450.

[34] Y. Mo, X. Zhao, and Y. Shen, Cation-dependent structural instability of graphene oxide membranes and its effect on membrane separation performance, Desalination 399 (2016) 40–46.

[35] J. Abraham, K. S. Vasu, C. D. Williams, K. Gopinadhan, Y. Su, C. T. Cherian, J. Dix, E. Prestat, S. J. Haigh, I. V. Grigorieva, P. Carbone, A. K. Geim and R. R. Nair, Tunable sieving of ions using graphene oxide membranes, Nat. Nanotechnol. 12 (2017) 546–550.

[36] Y. Zhang, S. Zhang, and T. S. Chung, Nanometric graphene oxide framework membranes with enhanced heavy metal removal via nanofiltration, Environ. Sci. Technol. 49 (2015) 10235–10242.

[37] M. Hu and B. Mi, Layer-by-layer assembly of graphene oxide membranes via electrostatic interaction, J. Memb. Sci. 469 (2014) 80–87.

[38] J. J. Richardson, J. Cui, M. Björnmalm, J. A. Braunger, H. Ejima, and F. Caruso, Innovation in layer-by-layer assembly, Chem. Rev. 116 (2016) 14828–14867.

[39] Q. Nan, P. Li, and B. Cao, Fabrication of positively charged nanofiltration membrane via the layer-by-layer assembly of graphene oxide and polyethylenimine for desalination, Appl. Surf. Sci. 387 (2016) 521–528.

[40] W. Choi, J. Choi, J. Bang, and J. H. Lee, Layer-by-layer assembly of graphene oxide nanosheets on polyamide membranes for durable reverse-osmosis applications, ACS Appl. Mater. Interfaces 5 (2013) 12510–12519.

[41] O. Sanli, Homogeneous hydrolysis of polyacrylonitrile by potassium hydroxide, Eur. Polym. J. 26 (1990) 9–13.

[42] M. Jassal, S. Bhowmick, S. Sengupta, P. K. Patra, and D. I. Walker, "Hydrolyzed poly(acrylonitrile) electrospun ion-exchange fibers," Environ. Eng. Sci. 31 (2014) 288–299.

[43] X. Liu, N. Wen, X. Wang, and Y. Zheng, "Layer-by-layer self-assembled graphene multilayer films via covalent bonds for supercapacitor electrodes, Nanomater. Nanotechnol. 5 (2015) article number 14.

[44] M. I. Verkhovsky, A. Jasaitis, M. L. Verkhovskaya, J. E. Morgan, and M. Wikström, Proton translocation by cytochrome c oxidase., Nature 400 (1999) 480–483.

[45] M. Frasconi, R. Tel-vered, J. Elbaz, and I. Willner, Electrochemically-stimulated pH changes : A route to control chemical reactivity, J. Am. Chem. Soc. 132 (2010) 1–3.

[46] Z. Abdulagatova, I. M. Abdulagatov, and V. N. Emirov, "Effect of temperature and pressure on the thermal conductivity of sandstone," Int. J. Rock Mech. Min. Sci. 46 (2009) 1055–1071.

[47] M. M. Sk and C. Y. Yue, Layer-by-layer (LBL) assembly of graphene with p-phenylenediamine (PPD) spacer for high performance supercapacitor applications, RSC Adv. 4 (2014) 19908–19915.

[48] M. R. Acocella, C. E. Corcione, A. Giuri, M. Maggio, A. Maffezzoli, and G. Guerra, Graphene oxide as a catalyst for ring opening reactions in amine crosslinking of epoxy resins, RSC Adv. 6 (2016) 23858–23865.

[49] R. M. Silverstein, F. X. Webster, and D. J. Kiemle, Identification of organic compounds (Spectrometric Identification of Organic Compounds), 4th ed, Wiley, New York, 1981.

[50] N. P. G. Roeges, Guide to complete interpretation of infrared spectra of organis structures, Wiley and Sons Ltd, Chichester, 1994.

[51] C. Hontoria-Lucas, A. . Lopez-Peinado, de D. Lopez-Gonzalez, M. . Cervantes-Rojas, and R. . Martin-Aranda, Study of oxygen containing groups in a series of graphite oxides: Physical and Chemical Characterization, Carbon 33 (1995) 1585-1592.

[52] J. I. Paredes, A. Martı, and J. M. D. Tascon, Graphene oxide dispersions in organic solvents, Langmuir 24 (2008) 10560-10564.

[53] Y. Wei, Y. Zhang, X. Gao, Z. Ma, X. Wang, and C. Gao, Multilayered graphene oxide membrane for water treatment: A Review, Carbon 139 (2018) 964-981.

[54] W. R. Bowen and J. S. Welfoot, Modelling the performance of membrane nanofiltration-critical assessment and model development, Chem. Eng. Sci. 57 (2002) 1121–1137.

[55] A. Czapik, H. Konowalska, and M. Gdaniec, "P-Phenyl-enediamine and its dihydrate: Two-dimensional isomorphism and mechanism of the dehydration process, and N-H···N and N-H···π interactions," Acta Crystallogr. Sect. C Cryst. Struct. Commun. 66 (2010) 128–132.

[56] A. J. Wu, X. D. Li, J. Yang, and J. H. Yan, Synthesis and characterization of a plasma carbon aerosol coated sponge for recyclable and efficient separation and adsorption, RSC Adv. 7 (2017) 9303–9308.

[57] F. Renate, S. Holger, and J. Tobias, Surface Design: Applications in Biosciences and Nanotechnology, Wiley-VCH, 2009.

[58] W. S. Hung et al., Cross-linking with diamine monomers to prepare composite graphene oxide-framework membranes with varying d-spacing, Chem. Mater. 26 (2014) 2983–2990.

[59] N. F. D. Aba, J. Y. Chong, B. Wang, C. Mattevi, and K. Li, Graphene oxide membranes on ceramic hollow fibers - microstructural stability and nanofiltration performance, J. Memb. Sci. 484 (2015) 87–94.

[60] J. de S. Macedo et al., Kinetic and calorimetric study of the adsorption of dyes on mesoporous activated carbon prepared from coconut coir dust, J. Colloid Interface Sci. 298 (2006) 515–522.

[61] M. Oz, D. E. Lorke, M. Hasan, and G. A. Petroianu, Cellular and molecular actiones of methylene blue in the nervous system, Med Res Rev. 31 (2012) 93–117.

[62] M. J. S. Dewar, E. G. Zoebisch, E. F. Healy, and J. J. P. Stewart, Development and use of quantum mechanical molecular models. 76. AM1: a new general purpose quantum mechanical molecular model, J. Am. Chem. Soc. 107 (1985) 3902–3909.

[63] D. Qiuju, J. Sun, Y. Li, X. Yang, X. Wang, Z. Wang and L. Xia, Highly enhanced adsorption of congo red onto graphene oxide/chitosan fibers by wet-chemical etching off silica nanoparticles, Chem. Eng. J. 245 (2014) 99–106.

[64] L. Chen, Y. Li, S. Hu, J. Sun, D. Qiuju, X. Yang, Q. Ji, Z. Wang, D. Wang and Y. Xia, Removal of methylene blue from water by cellulose/graphene oxide fibres, J. Exp. Nanosci. 11 (2016) 1156–1170.

[65] Q. Ling, Z. Xuehua, Y. Wenrong, W. Yufei, S. George P, and L. Dan, Controllable corrugation of chemically converted graphene sheets in water and potential application for nanofiltration, Chem. Commun. 47 (2011) 5810–5812.

[66] M. Hu and B. Mi, Enabling graphene oxide nanosheets as water separation membranes, Environ. Sci. Technol. 47 (2013) 3715–3723.

[67] K. Viktor, W. Wilfried, and U. Mathias, Molecularly imprinted composite membranes for selective binding of desmetryn from aqueous solutions, Desalination 149 (2002) 323–326.

[68] W. Peng, H. Li, Y. Liu, and S. Song, Adsorption of methylene blue on graphene oxide prepared from amorphous graphite: Effects of pH and foreign ions, J. Mol. Liq. 221 (2016) 82-87.

[69] S. Yang, S. Chen, Y. Chang, A. Cao, Y. Liu and H. Wang, Removal of methylene blue from aqueous solution by graphene oxide, J. of Col. and Interface Science 359 (2011) 24-29.

[70] L. Ai, C. Zhang and Z. Chen, Removal of methylene blue from aqueous solution by a solvothermal-synthesized graphene/magnetite composite, J. of Hazardous Mat. 192 (2011) 1515-1524.

[71] M. Yuan, S. Tong, S. Zhao and C. Jia, Adsorption of polycyclic aromatic hydrocarbons from water using petroleum coke-derived porous carbo", J. Haz. Mats. 181 (2010) 1115-1120.

[72] D. Barreda, A.M. Perez-Mas, A. Silvestre-Albero, M.E. Casco, S. Rudic, C. Herdes, E.A. Müller, C. Blanco, R. Santamaría, J. Silvestre-Albero and F. Rodriguez-Reinoso, Unusual flexibility of mesophase pitch-derived carbon materials: An approach to the synthesis of graphene", Carbon 115 (2017) 539-545.

[73] W. P. Lee and A. F. Routh, Why Do Drying Films Crack?, Langmuir 20 (2004) 9885–9888.

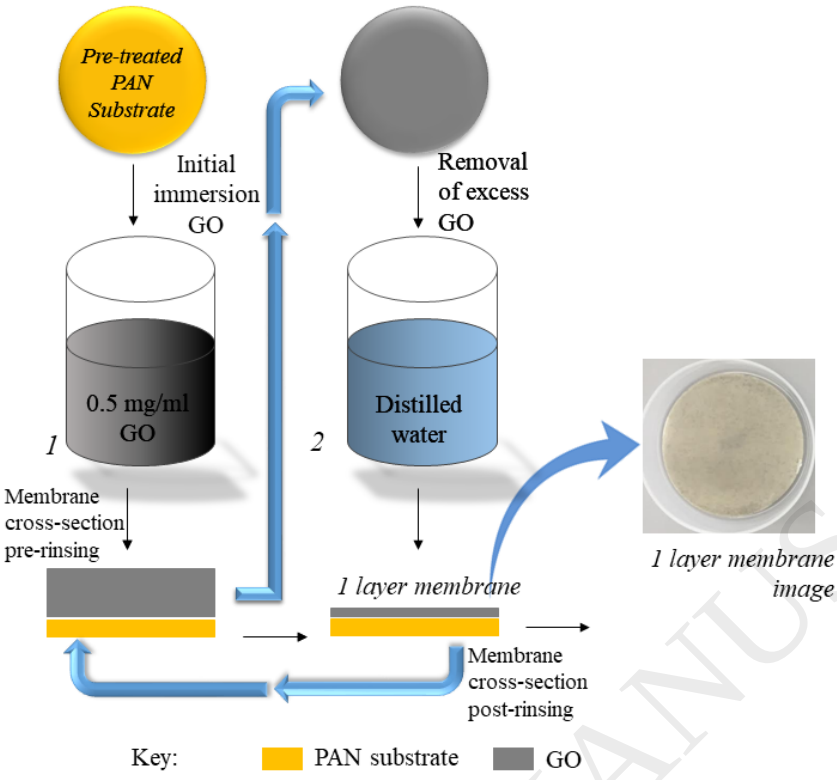

Figure 1. Dip-coating schematic (fabrication of uncrosslinked membranes).

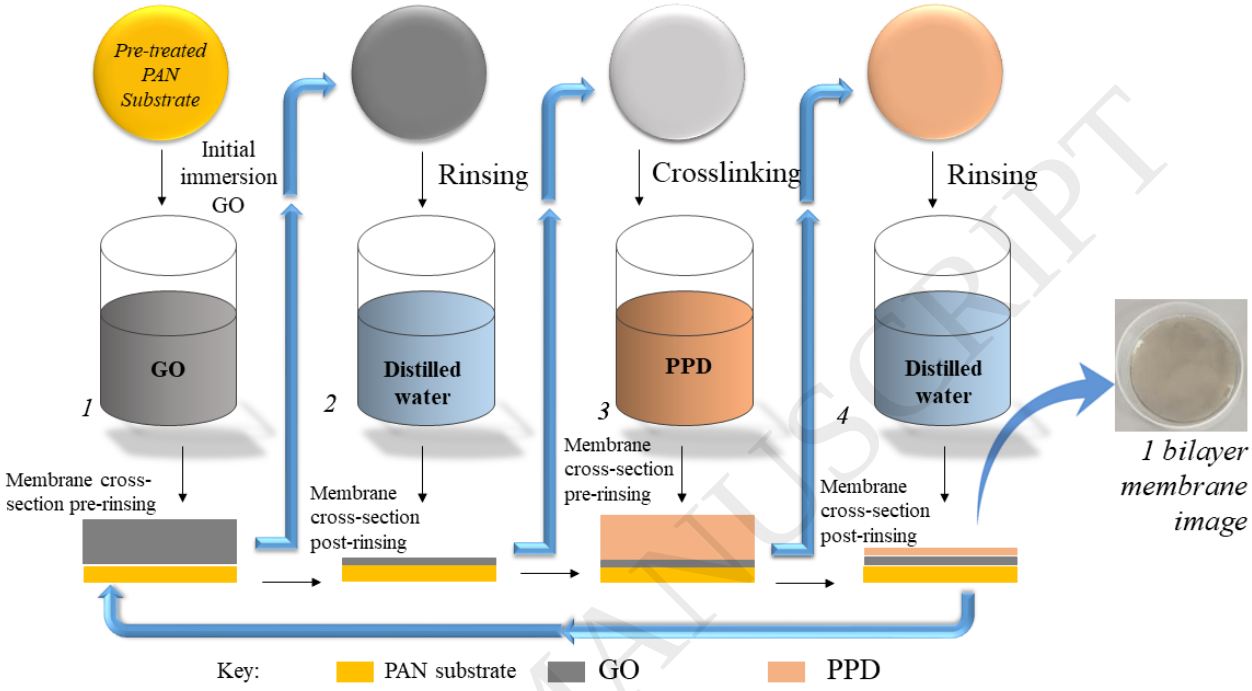

Figure 2. Dip-assisted layer-by-layer schematic (fabrication of crosslinked membranes).

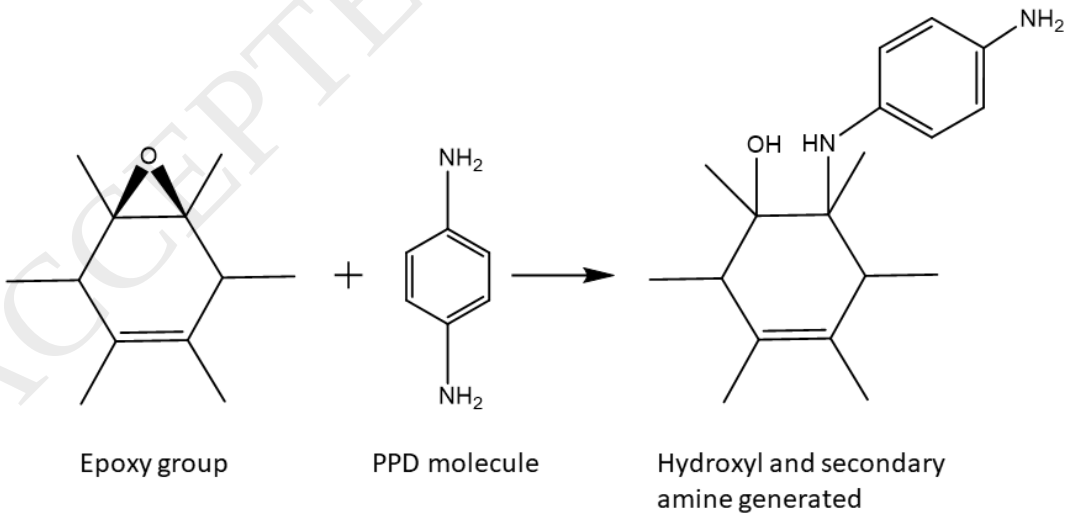

Figure 3. Epoxy ring opening reaction between GO and PPD.

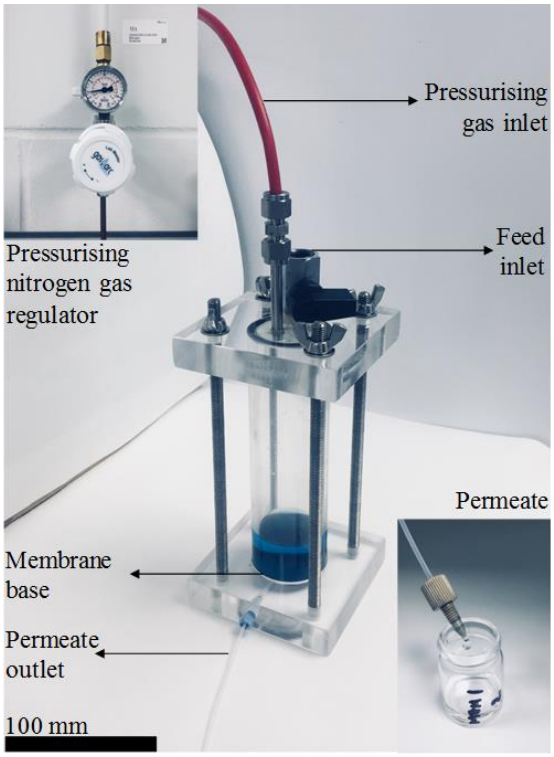

Figure 4. Homemade nanofiltration cell unit in operation.

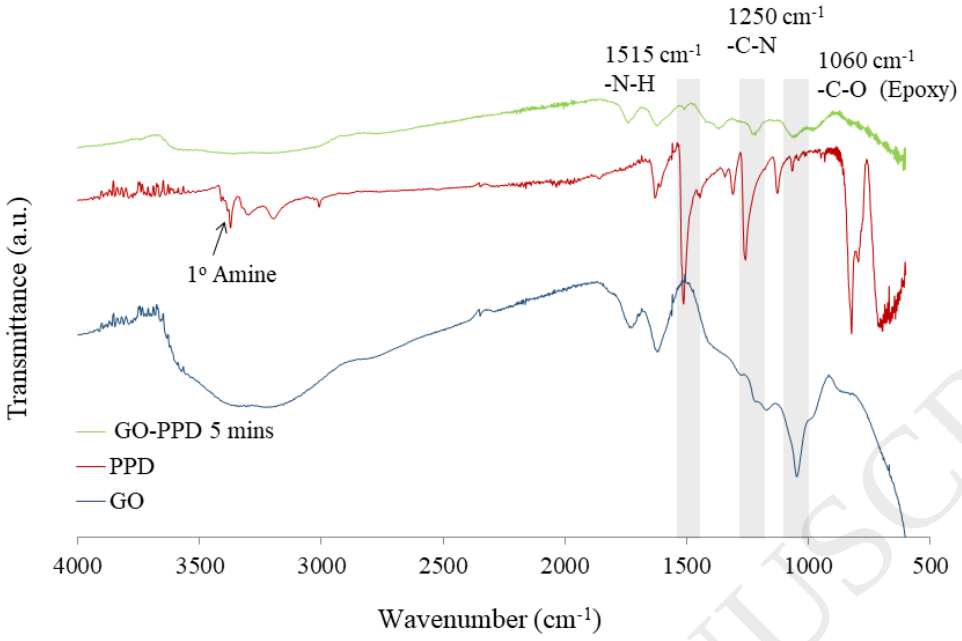

Figure 5. FTIR characterization of GO, PPD and GO-PPD reacted entity.

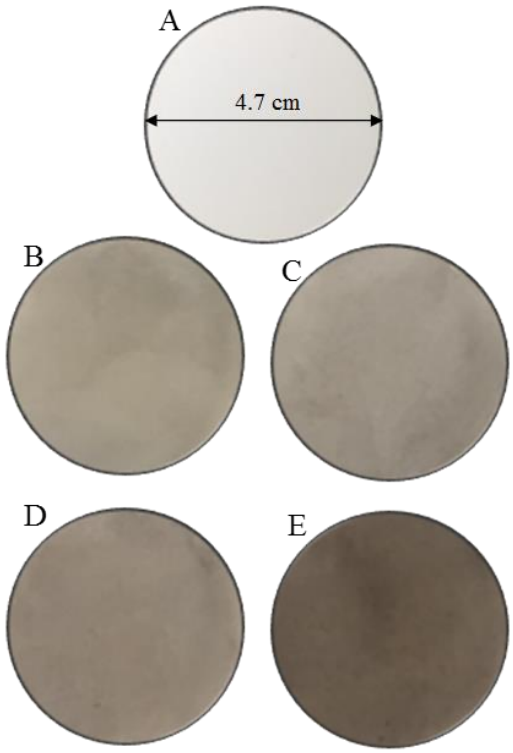

Figure 6. Photographic images of the fabricated membranes (pre-nanofiltration). A: Uncoated PAN substrate; B: Uncrosslinked membrane 1 layer; C: Crosslinked membrane 1 bilayer; D: Uncrosslinked membrane 5 layers; E: Crosslinked membranes 5 bilayers.

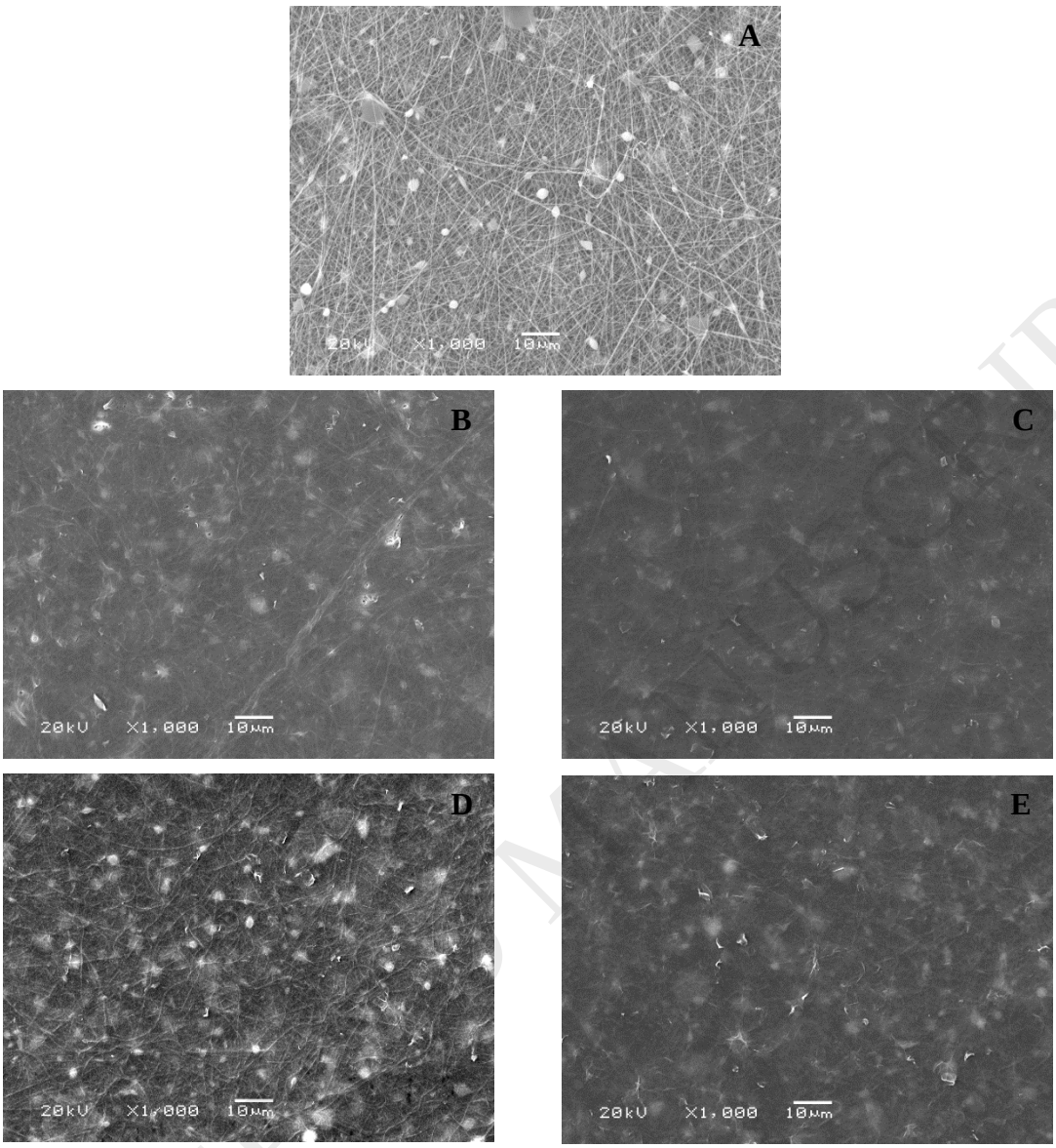

Figure 7. SEM images of the fabricated membranes (pre-nanofiltration). A: Uncoated PAN substrate; B: Uncrosslinked membrane 1 layer; C: Crosslinked membrane 1 bilayer; D: Uncrosslinked membrane 5 layers; E: Crosslinked membranes 5 bilayers.

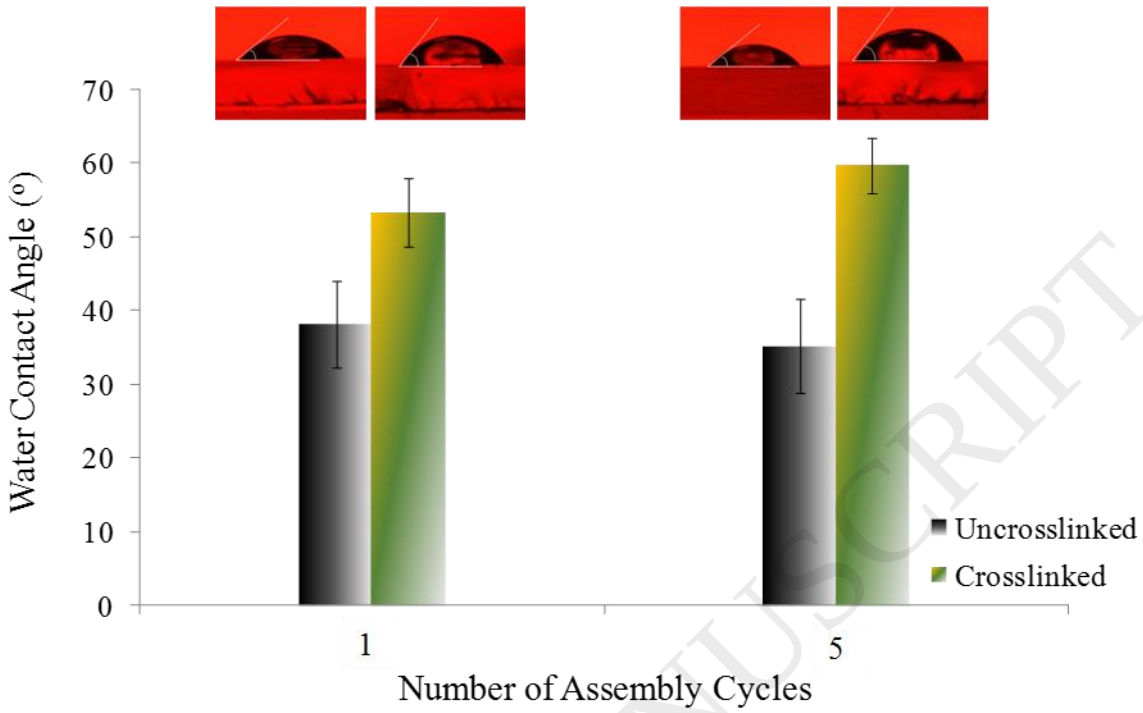

Figure 8. Water contact angles of the fabricated coatings

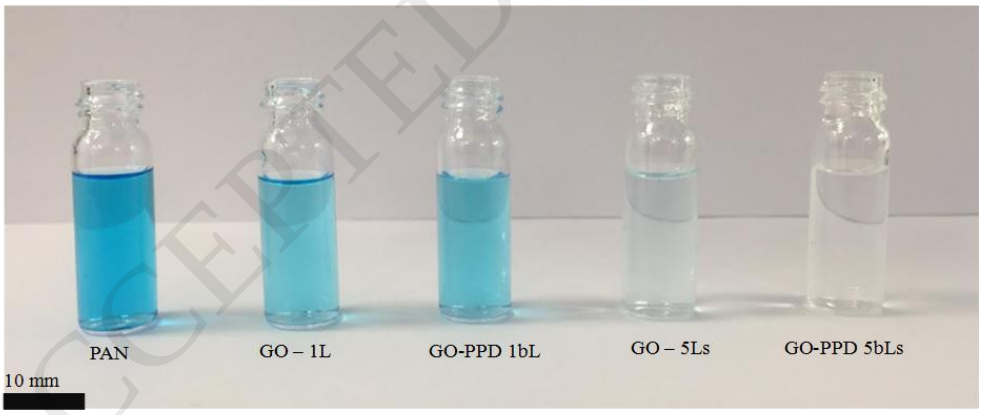

Figure 9. Nanofiltration permeates of each membrane.

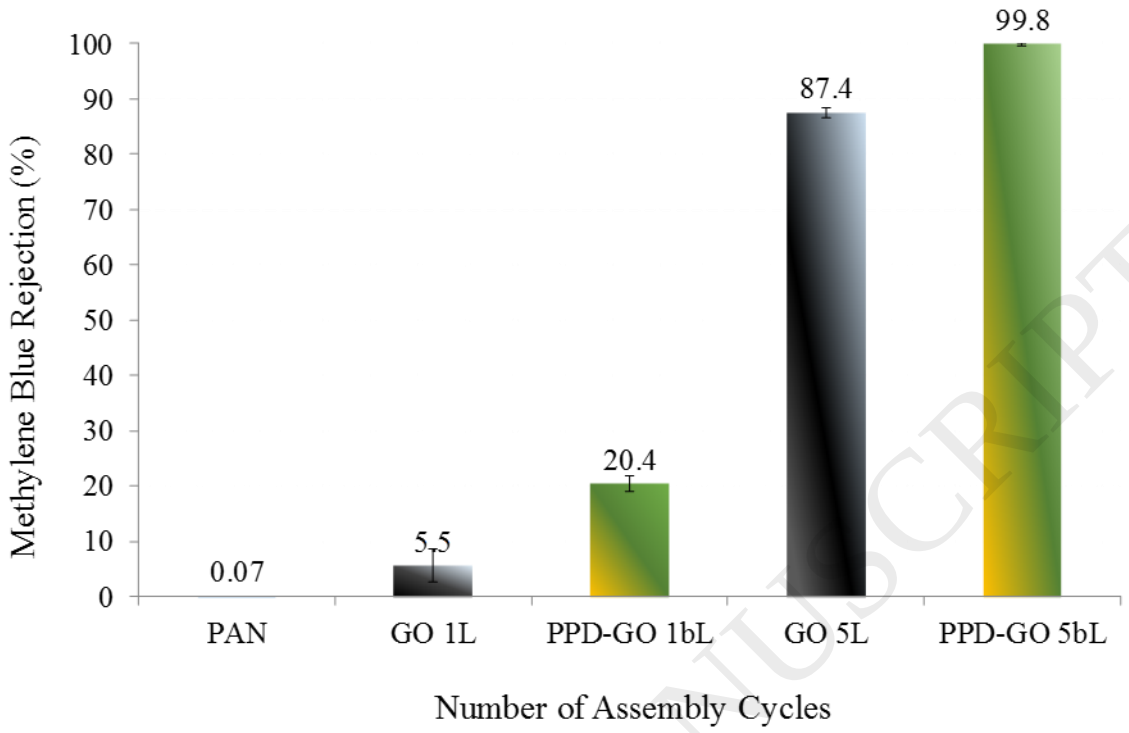

Figure 10. MB Rejection with respect to increase in the number of layers and bi-layers including plain PAN substrate.

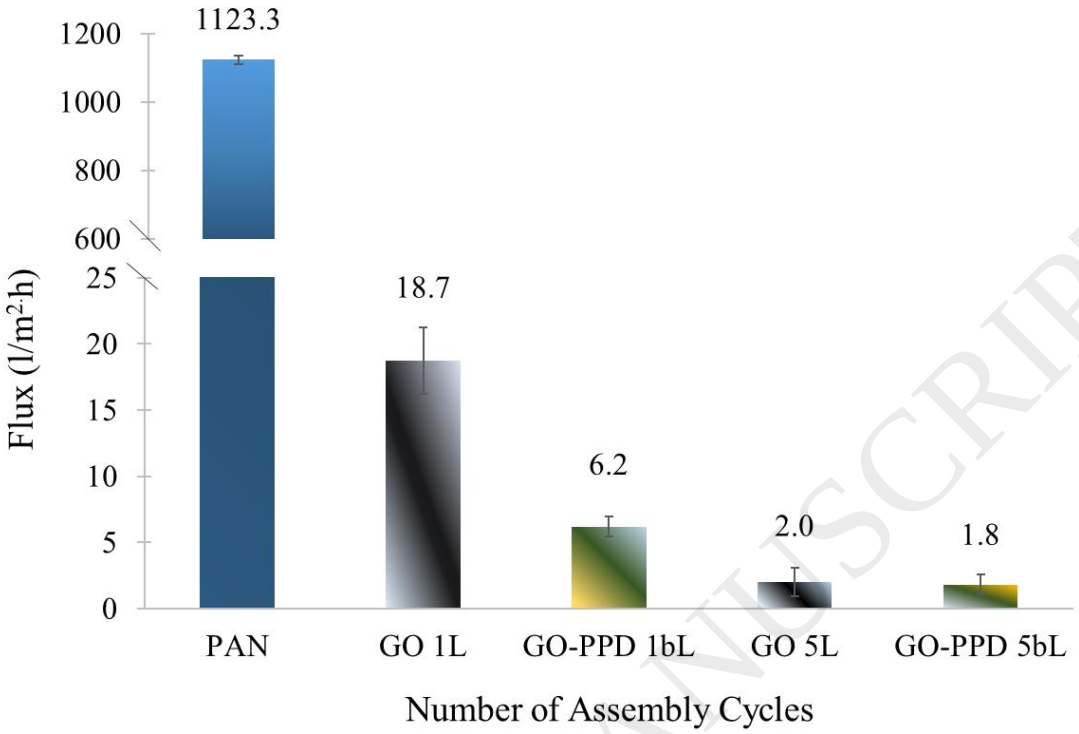

Figure 11. Permeation flux with respect to increase in the number of layers and bi-layers including plain PAN substrate.

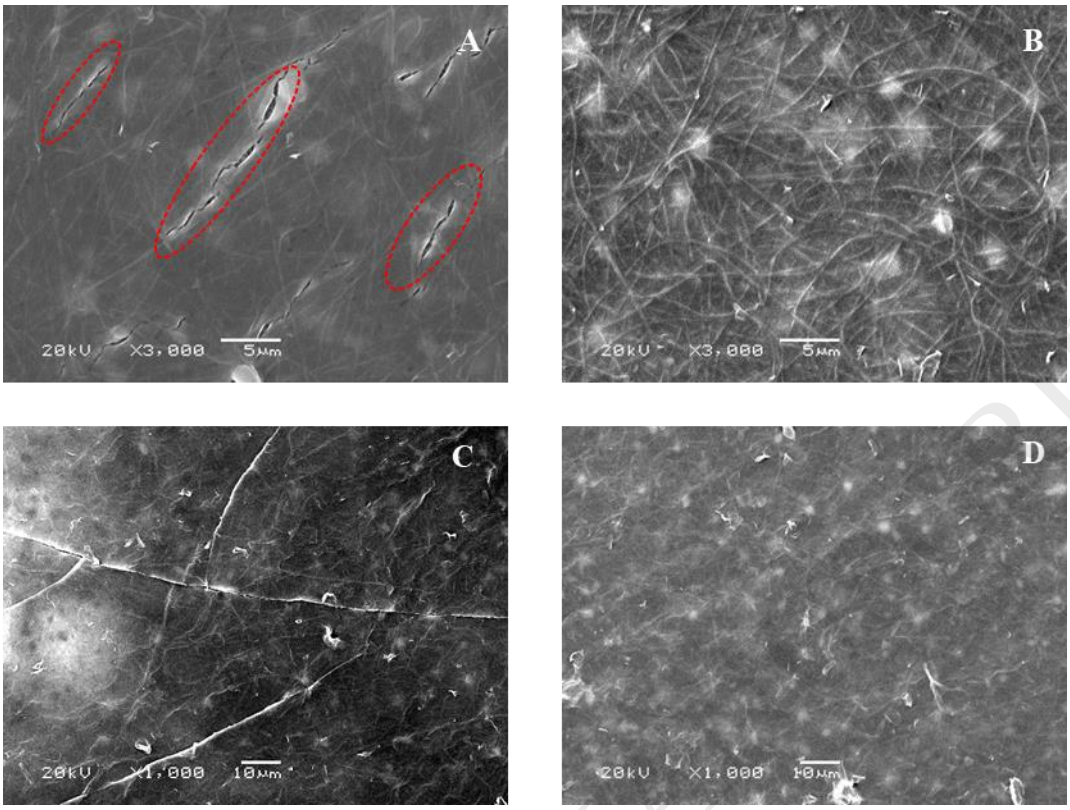

Figure 12. SEM images of the fabricated membranes (post-nanofiltration). A: Uncrosslinked membrane 1 layer; B: Crosslinked membrane 1 bilayer; C: Uncrosslinked membrane 5 layers; D: Crosslinked membranes 5 bilayers

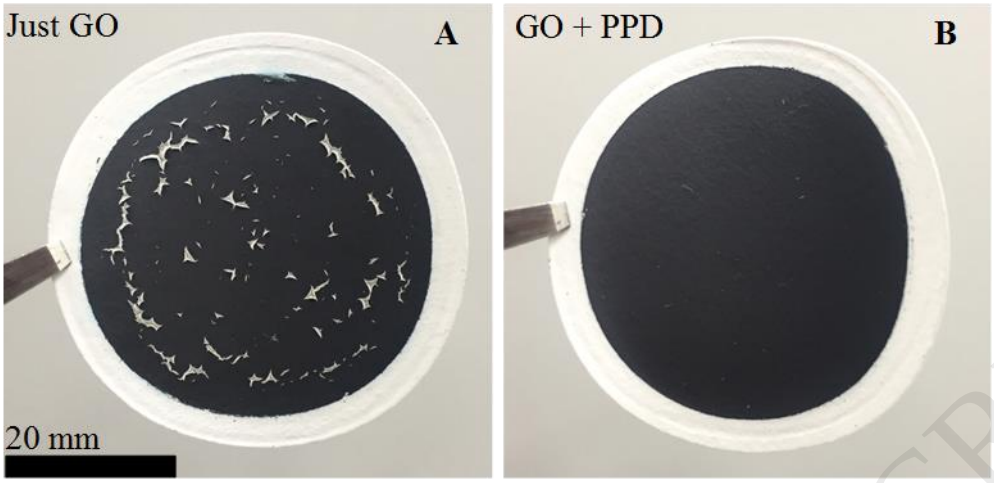

Figure 13. Pressure assisted fabricated membranes after drying. A: uncrosslinked membrane; B: PPD-crosslinked membrane.

Table 1. Surface chemistry of GO and GO-PPD reacted entity.

	GO	GO-PPD reacted 5 min
C 1s (at.%)	71.2	67.5
O 1s (at.%)	27.4	29.9
S 1s (at.%)	1.3	1.6
N 1s (at.%)	---	1.0
Csp2 (%)	54.8	45.7
Csp3 (%)	3.7	6.2
C(epoxy) (%)	37.1	25.7
C=O (%)	1.2	15.7
COOH (%)	3.2	6.3
π-π* (%)	0.0	0.5
N6 (%)	---	17.6
NC (%)	---	26.4
N5 (%)	---	6.7
NQ (%)	---	39.0
N-X (%)	---	10.3

Table 2. Membrane separation rejection for the 5 bi-layers crosslinked membrane at prolonged operation hours (working pressure 1 bar) and 10 mg/l MB.

Operation time (h)	MB rejection (%)	Permeation flux ($l.m^{-2}.h^{-1}$)
10	99.8	1.81
20	100.0	1.47
45	100.0	0.85
70	100.0	0.63
108	100.0	0.41
121	100.0	0.36

Table 3. Relation between increasing feed concentration and membrane performance at lower and higher operation times (5 bi-layers crosslinked membrane).

Feed concentration (mg/l)	MB rejection (%) after		Permeation flux ($l.m^{-2}.h^{-1}$) after	
	3 hours	20 hours	3 hours	20 hours
10	99.8	100	1.81	1.47
125	98.3	100	0.81	0.43
250	96.7	98.1	0.23	0.07